

Dual-channel tunable near-infrared absorption enhancement with graphene induced by coupled modes of topological interface states

Zeng-Ping Su(苏增平), Tong-Tong Wei(魏彤彤), and Yue-Ke Wang(王跃科)
Citation: Chin. Phys. B, 2022, 31 (**8**): 087804. DOI: 10.1088/1674-1056/ac6744
Journal homepage: http://cpb.iphy.ac.cn; http://iopscience.iop.org/cpb

What follows is a list of articles you may be interested in

Tunable wide-angle multi-band mid-infrared linear-to-linear polarization converter based on a graphene metasurface

Lan-Lan Zhang(张兰兰), Ping Li(李萍), and Xiao-Wei Song(宋霄薇)
Chin. Phys. B, 2021, 30 (**12**): 127803. DOI: 10.1088/1674-1056/ac0cdd

Faraday rotations, ellipticity, and circular dichroism in magneto-optical spectrum of moiré superlattices

J A Crosse and Pilkyung Moon
Chin. Phys. B, 2021, 30 (**7**): 077803. DOI: 10.1088/1674-1056/ac051f

Enhanced microwave absorption performance of MOF-derived hollow Zn-Co/C anchored on reduced graphene oxide

Yue Wang(王玥), Dawei He(何大伟), and Yongsheng Wang(王永生)
Chin. Phys. B, 2021, 30 (**6**): 067804. DOI: 10.1088/1674-1056/abd770

Plasmonic properties of graphene on uniaxially anisotropic substrates

Shengchuan Wang(汪圣川), Bin You(游斌), Rui Zhang(张锐), Kui Han(韩奎), Xiaopeng Shen(沈晓鹏, and Weihua Wang(王伟华)
Chin. Phys. B, 2021, 30 (**3**): 037801. DOI: 10.1088/1674-1056/abd168

Modulation of the second-harmonic generation in MoS_2 by graphene covering

Chunchun Wu(吴春春), Nianze Shang(尚念泽), Zixun Zhao(赵子荀), Zhihong Zhang(张智宏), Jing Liang(梁晶), Chang Liu(刘畅), Yonggang Zuo(左勇刚), Mingchao Ding(丁铭超), Jinhuan Wang(王金焕), Hao Hong(洪浩), Jie Xiong(熊杰), and Kaihui Liu(刘开辉)
Chin. Phys. B, 2021, 30 (**2**): 027803. DOI: 10.1088/1674-1056/abd77f

---

Dual-channel tunable near-infrared absorption enhancement with graphene induced by coupled modes of topological interface states

Zeng-Ping Su(苏增平)[1,2], Tong-Tong Wei(魏彤彤)[1,2], and Yue-Ke Wang(王跃科)[1,2,†]

[1] *Optical Information Science and Technology Department, Jiangnan University, Wuxi* 214122, *China*
[2] *Optoelectronic Engineering and Technology Research Center, Jiangnan University, Wuxi* 214122, *China*

(Received 6 October 2021; revised manuscript received 27 March 2022; accepted manuscript online 14 April 2022)

The dual-channel nearly perfect absorption is realized by the coupled modes of topological interface states (TIS) in the near-infrared range. An all-dielectric layered heterostructure composed of photonic crystals (PhC)/graphene/PhC/graphene/PhC on GaAs substrate is proposed to excite the TIS at the interface of adjacent PhC with opposite topological properties. Based on finite element method (FEM) and transfer matrix method (TMM), the dual-channel absorption can be modulated by the periodic number of middle PhC, Fermi level of graphene, and angle of incident light (TE and TM polarizations). Especially, by fine-tuning the Fermi level of graphene around 0.4 eV, the absorption of both channels can be switched rapidly and synchronously. This design is hopefully integrated into silicon-based chips to control light.

Keywords: one-dimensional photonic crystals, graphene, topological interface states

PACS: 78.67.Pt, 42.70.Qs, 42.25.Bs, 78.67.Wj **DOI:** 10.1088/1674-1056/ac6744

1. Introduction

Photonic crystals (PhC), as an artificial periodic dielectric material with periodicity in one, two or all three orthogonal directions, have been intensively investigated since Yablonovitch[1] and John[2] independently proposed the concept of PhC in 1989.[3] Similar to the electronic band gaps in semiconductor, PhC can prohibit electromagnetic waves in some specific frequency zones called the photonic band gaps.[4–6] In recent years, the studies of photonic topological insulators have attracted much attention due to their extraordinary properties including the elimination of backscattering and immunity to structural disorder.[7–9] Particularly, topologically protected edge states in PhC show broad prospects in the application of integrated photonic circuits and ultrahigh-speed information processing chips.[10] For one-dimensional (1D) PhC system, topological interface states (TIS) exist at the interface of the adjacent PhC with different topological properties. The existence of TIS can generate a sharp transmission peak within the photonic band gaps and a highly localized electric field around the interface,[11,12] which is promising to be used to enhance the light–matter interactions.[13]

Graphene has been demonstrated as a good candidate for photonic and optoelectronic devices due to its unique characteristics, including the ultrahigh charge carrier mobility, extremely wide spectral range, and dynamical tunability via external doping or bias voltage.[14] In the range from mid- to far-infrared, the optical properties of graphene are similar to those of Drude-type materials, and strong resonance absorption can be achieved through plasmonic resonance.[15–18] However, graphene is almost transparent with an absorptivity of 2.3% in the visible and near-infrared range,[19] which largely limits its substantial application in photon detection and photoelectric conversion.[20] To overcome such shortcomings, optical interface states, such as Tamm plasmon polaritons (TPP) and TIS, can be introduced to enhance the light absorption of monolayer graphene.[21–29] For TIS and TPP, strong field localization can be realized at interface, which plays an extremely important role in the enhanced absorption of graphene. The strong field localization strengthens the interaction between graphene and incident light; thus, the higher absorption efficiency can be achieved. Lu *et al*. numerically and theoretically investigated high-efficiency light absorption of monolayer graphene via TPP in the near-infrared range.[21] Wang *et al*. achieved multichannel terahertz perfect absorber by TPP in the far-infrared range.[22] Lin *et al*. theoretically presented a tunable light absorption of graphene using TIS in visible range.[28] Also in visible range, Hu *et al*. theoretically accomplished dual-band absorption enhancement by strong coupling of TPP and TIS in 1D topological PhC heterostructure/Ag hybrid system.[24] Nevertheless, the near-infrared absorption enhancement with graphene through the coupled modes of TIS in all-dielectric topological PhC heterostructure system has not been reported.

In this work, we propose to achieve dual-channel absorption enhancement with graphene by the all-dielectric topological PhC heterostructure in the near-infrared range. The monolayer graphene is placed at the interface of adjacent PhC with opposite topological properties, where TIS can be excited. The dual-channel nearly perfect absorption can be obtained due to

†Corresponding author. E-mail: ykwang@jiangnan.edu.cn
© 2022 Chinese Physical Society and IOP Publishing Ltd

the coupled modes of TIS. We numerically and theoretically analyze the influence of pairs number of PhC in the center and incident angle (TE and TM polarizations) on the dual-channel absorption curves based on finite element method (FEM) and transfer matrix method (TMM), respectively. Besides, the dual-channel optical switches can be realized by controlling the Fermi level of graphene.

2. Results and discussion

As shown in Fig. 1, the structure used to realize the coupled modes of TIS is composed of PhC-F (alternating $N_{\rm F}$ (= 4) pairs of Si/SiO_2/Si)/graphene/PhC-M (alternating $N_{\rm M}$ (= 2) pairs of SiO_2/Si/SiO_2)/graphene/PhC-B (alternating $N_{\rm B}$ (= 8) pairs of Si/SiO_2/Si) on a GaAs substrate. A plane wave of TM polarization (magnetic field is perpendicular to the x–z plane) or TE polarization (electric field is perpendicular to the x–z plane) is incident on the proposed structure from surrounding medium (Si) along the positive z axis with an incident angle θ in x–z plane. Here, the parameters of the proposed structure are $a_1 = 690$ nm, $b_1 = 822$ nm, $a_2 = 205$ nm, $b_2 = 170$ nm, and $d_{\rm s} = 2000$ nm for GaAs substrate. The parameters of PhC-F and PhC-B are the same, except for the number of pair ($N_{\rm F}$ and $N_{\rm B}$). The refractive indices of Si, SiO_2, and GaAs are $n_{\rm a} = 2.82$, $n_{\rm b} = 1.46$ and $n_{\rm s} = 3.4$, respectively.[10,30] We set the thickness of monolayer graphene $d_{\rm g} = 0.35$ nm. The surface conductivity of monolayer graphene is $\sigma_{\rm g}$, which is calculated according to the Kubo formula[25,31]

$$\sigma_{\rm g} = \frac{{\rm i}e^2E_{\rm f}}{\pi\hbar^2(\omega+{\rm i}\tau^{-1})} + \frac{{\rm i}e^2}{4\pi\hbar}{\rm Ln}\left[\frac{2E_{\rm f}-(\omega+{\rm i}\tau^{-1})\hbar}{2E_{\rm f}+(\omega+{\rm i}\tau^{-1})\hbar}\right] + \frac{{\rm i}2e^2k_{\rm B}T}{\pi\hbar^2(\omega+{\rm i}\tau^{-1})}{\rm Ln}\left[\exp\left(-\frac{E_{\rm f}}{k_{\rm B}T}\right)+1\right], \quad (1)$$

where $E_{\rm f}$ is the Fermi level, τ is electron–phonon relaxation time, e is the charge of an electron, $k_{\rm B}$ is the Boltzmann's constant, ω is the radian frequency, and $\hbar$ is the reduced Planck's constant. The permittivity $\varepsilon_{\rm g}$ of graphene can be written as $\varepsilon_{\rm g} = 1 + {\rm i}\sigma_{\rm g}\eta/(kd_{\rm g})$, where η (= 377 Ω) is the impedance of air. Here, the Fermi level $E_{\rm f}$ is 0.2 eV, T is 300 K, relaxation time τ is $\mu E_{\rm f}/(ev_{\rm f}^2)$, DC mobility μ is 10000 $cm^2/V{\cdot}s$, and Fermi velocity $v_{\rm f}$ is 1×10^6 m/s.

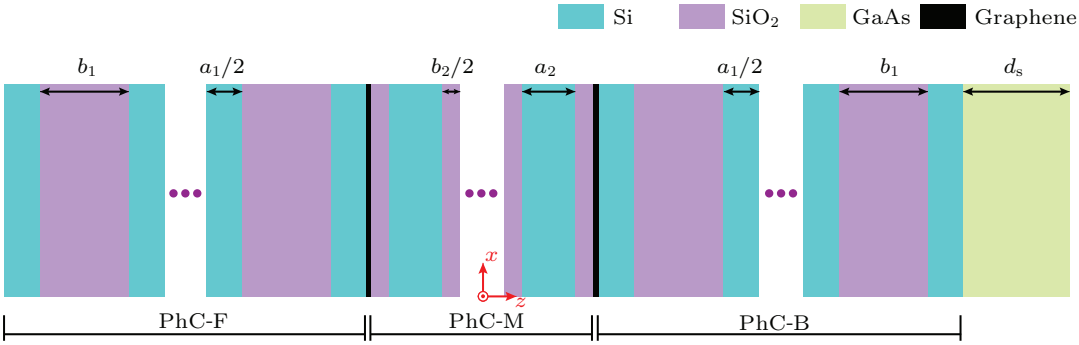


Fig. 1. Schematic diagram of the 1D all-dielectric PhC heterostructure consisting of PhC-F/graphene/PhC-M/graphene/PhC-B on a GaAs substrate. In each unit cell, a single layer of SiO_2 (or Si) is sandwiched between half layers of Si (or SiO_2) for PhC-F(B) (or PhC-M). And the light illuminates from surrounding medium (Si) along the positive z axis.

The band structures of PhC-F(B) and PhC-M are shown in Figs. 2(a) and 2(b) for the on-axis propagation, respectively. The Zak phase (0 or π) of m-th isolated band can be calculated by[32]

$$\theta_m^{\rm Zak} = \int_{\rm BZ}\left[{\rm i}\int_{\text{unit cell}}\varepsilon(z)u_{m,q}^*(z)\partial_q u_{m,q}(z){\rm d}z\right]{\rm d}q, \quad (2)$$

where BZ refers to Brillouin zone, $\varepsilon(z)$ is space permittivity, and $u_{m,q}(z)$ denotes the Bloch eigenfunction of electric field at the m-th isolated band. Here, the Zak phase of the lowest 0th band can be obtained by $\exp\left({\rm i}\theta_0^{\rm Zak}\right) = {\rm sgn}\left[1-(\varepsilon_{\rm b}\mu_{\rm a})/(\varepsilon_{\rm b}\mu_{\rm a})\right]$, where $\varepsilon_{\rm a}$, $\varepsilon_{\rm b}$ and $\mu_{\rm a}$, $\mu_{\rm b}$ are the relative permittivity and permeability, respectively. For nonmagnetic dielectric materials ($\mu_{\rm a} = \mu_{\rm b} = 1$), when the inversion center of the PhC has a low refractive index ($\varepsilon_{\rm a} < \varepsilon_{\rm b}$), $\theta_0^{\rm Zak}$ is 0; on the contrary ($\varepsilon_{\rm a} > \varepsilon_{\rm b}$), $\theta_0^{\rm Zak}$ is π. The Zak phase at higher band can be determined by the condition $\sin(2\pi n_i d_i/\lambda) = 0$, where λ is the wavelength, n_i and d_i (i = a or b) represent the refractive index and length of inversion center slab, respectively. The Zak phase $\theta_m^{\rm Zak}$ ($m > 1$) will be π if λ falls in the band; otherwise, it will be 0.[33] The Zak phase of each band is marked by green number for PhC-F(B) and PhC-M in Figs. 2(a) and 2(b). The topological properties of n-th gap can be determined by ${\rm sgn}\left[(-1)^n(-1)^l\exp\left({\rm i}\sum_{m=0}^{n-1}\theta_m^{\rm Zak}\right)\right]$, where the integer l is the number of crossing points under n-th gap.[32] The positive and negative topological properties of each gap are represented by magenta and blue, respectively. It has been confirmed that the TIS will appear at the interface of the adjacent PhC, when the gaps of the adjacent PhC with opposite topological properties have overlap frequency region.[34] According to Figs. 2(a) and 2(b), the 4th gap of PhC-F(B) and the 1th gap of PhC-M have opposite topological properties and a good overlap (corresponding to wavelength range of 1500–1655 nm), so the TIS and highly localized electric field can be generated at the interfaces of PhC-F/PhC-M and PhC-M/PhC-B. When

the thickness of PhC-M is thin enough ($N_M = 2$), the coupling between the two TIS at the interfaces of PhC-F/PhC-M and PhC-M/PhC-B can occur, and the coupled modes of TIS are excited. Here, the coupled modes of TIS are actually a conceptual extension of the TIS. The PhC-M shows opposite signs of the reflection phases to the PhC-F and PhC-B. This leads to coupling of TIS and consequently to mode splitting in overlap band gaps.[35]

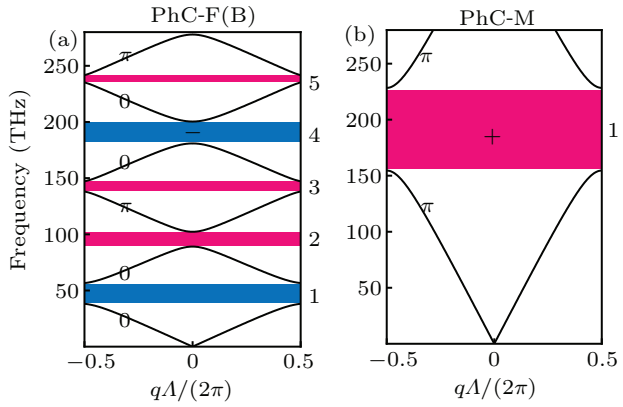


Fig. 2. Photonic band structure for PhC-F(B) (a) and PhC-M (b).

In this work, all numerical simulation results are obtained by the commercial software COMSOL Multiphysics based on FEM, and the periodic boundary condition are set in the x direction. In addition, we theoretically analyze the propagation features of the proposed all-dielectric PhC heterostructure by TMM.[36] Figure 3(a) shows the absorption and reflection curves for TE polarization at normal incidence ($\theta = 0°$) with (solid lines) and without (dots) graphene layer. It can be found that two absorption peaks appear for the PhC heterostructure with graphene layer, corresponding to the absorption value of 96.7% at 1564.8 nm and 97.9% at 1632 nm. However, the absorption is almost zero, and the two reflection valleys also appear at 1564.8 nm and 1632 nm for the PhC heterostructure without graphene layer. It is believed that the two absorption peaks in the PhC heterostructure with graphene layer are attributed to the excitation of the coupled modes of TIS. And the full width at half maximum (FWHM) of two absorption peaks are 1.6 nm and 3 nm, respectively. According to the definition of quality factor (Q), i.e., $\lambda/\Delta\lambda$, we obtain the quality factors for two absorption peaks, which are 978 at 1564.8 nm and 544 at 1534.6 nm, respectively. To illustrate the coupled modes of TIS, the calculated electric field distribution of E_y and profile of $|E_y|^2$ at 1564.8 nm and 1632 nm are shown in Figs. 3(b) and 3(c), respectively. Obviously, the field and energy are mainly localized near the interfaces of PhC-F/PhC-M and PhC-M/PhC-B, which are also the position of the graphene layers. In addition, the calculated electric field distribution of E_y is antisymmetric about the center of PhC-M ($z = 0$ nm) in Fig. 3(b), and the calculated electric field distribution (E_y) is symmetric about the center of PhC-M ($z = 0$ nm) in Fig. 3(c). Because the two TIS can be excited at the interfaces of PhC-F/PhC-M and PhC-M/PhC-B, the TIS generated at the two interfaces can couple with each other, resulting in coupled modes of TIS, named anti-symmetric mode (the absorption peak at 1564.8 nm) and symmetric mode (the absorption peak at 1632 nm), respectively. Due to the coupled modes of TIS, the highly localized electric field and energy at the interface enhance the interaction between light and graphene, and the dual-channel near-infrared absorption is achieved. Then, we study the influence of N_M (the pair numbers of PhC-M) on TIS-TIS coupling, as shown in Fig. 3(e). We calculate the absorption curves when N_M is 2, 3, 4, 7, and 10 based on FEM (black lines) and TMM (red dots). Clearly, as N_M increases, the absorption peaks corresponding to the coupled modes of TIS (anti-symmetric and symmetric modes) gradually move closer, and only a perfect absorption peak remains when $N_M = 10$. Figure 3(d) shows electric field distribution of E_y and profile of $|E_y|^2$ at absorption peak (1601.7 nm) corresponding to the absorption value of 99.9% and Q of 517 when $N_M = 10$. For our proposed all-dielectric PhC heterostructure with smaller N_M, the two TIS at the two interfaces can more strongly interact with each other, which leads to greater splitting for the coupled modes of TIS in wavelength regime. On the contrary, the interaction between TIS at the two interfaces gradually weakens, the two coupled modes of TIS gradually move closer. When $N_M = 10$, the interaction between TIS almost disappears and light is completely absorbed at the interface of PhC-F/PhC-M due to TIS, so only one absorption peak is retained. Thus, owing to the coupled modes of TIS, the dual-channel absorption enhancement with graphene can be achieved, and the dual-channel absorption enhancement can be adjusted by changing N_M. When N_M is large enough ($N_M = 10$), the single channel perfect absorption can also be achieved.

The effect of the Fermi level of graphene (E_f) on the dual-band enhancement absorption is also investigated. The imaginary parts of permittivity of graphene with Fermi level and wavelength are calculated as shown in Fig. 4(a). Obviously, When Fermi level is around 0.4 eV, the imaginary parts of permittivity of graphene will rapidly change from 17 to 0 as Fermi level increases. It leads to a rapid decay of absorption. Fermi level E_f can be actively changed by chemical doping and electrical or thermal stimulation.[37] Figures 4(b) and 4(c) depict absorption of numerical simulation as a function of the wavelength and E_f at normal incidence ($\theta = 0°$) when $N_M = 2$ and 4, respectively. It can be clearly observed that absorption does not have significant variations at E_f of less than 0.4 eV, but when E_f is slightly greater than 0.4 eV, the absorption experiences a significant drop. This is consistent with the result obtained by Fig. 4(a). As shown in the insets in Figs. 4(b) and 4(c), when E_f increases from 0.36 eV to 0.42 eV, the peak

absorption for wavelength 1564.8 nm, 1632 nm, 1591.3 nm and 1611.3 nm drops from 93.1% to 6.5%, 96.5% to 7.4%, 90.1% to 6.8%, and 92.8% to 7.1%, respectively. It means that the dual-channel absorption can be rapidly adjusted at the same time by changing E_f around 0.4 eV. This phenomenon is valuable for many practical applications, including optical switches, modulators, etc. Besides, the working wavelength can also be selected by adjusting N_M.

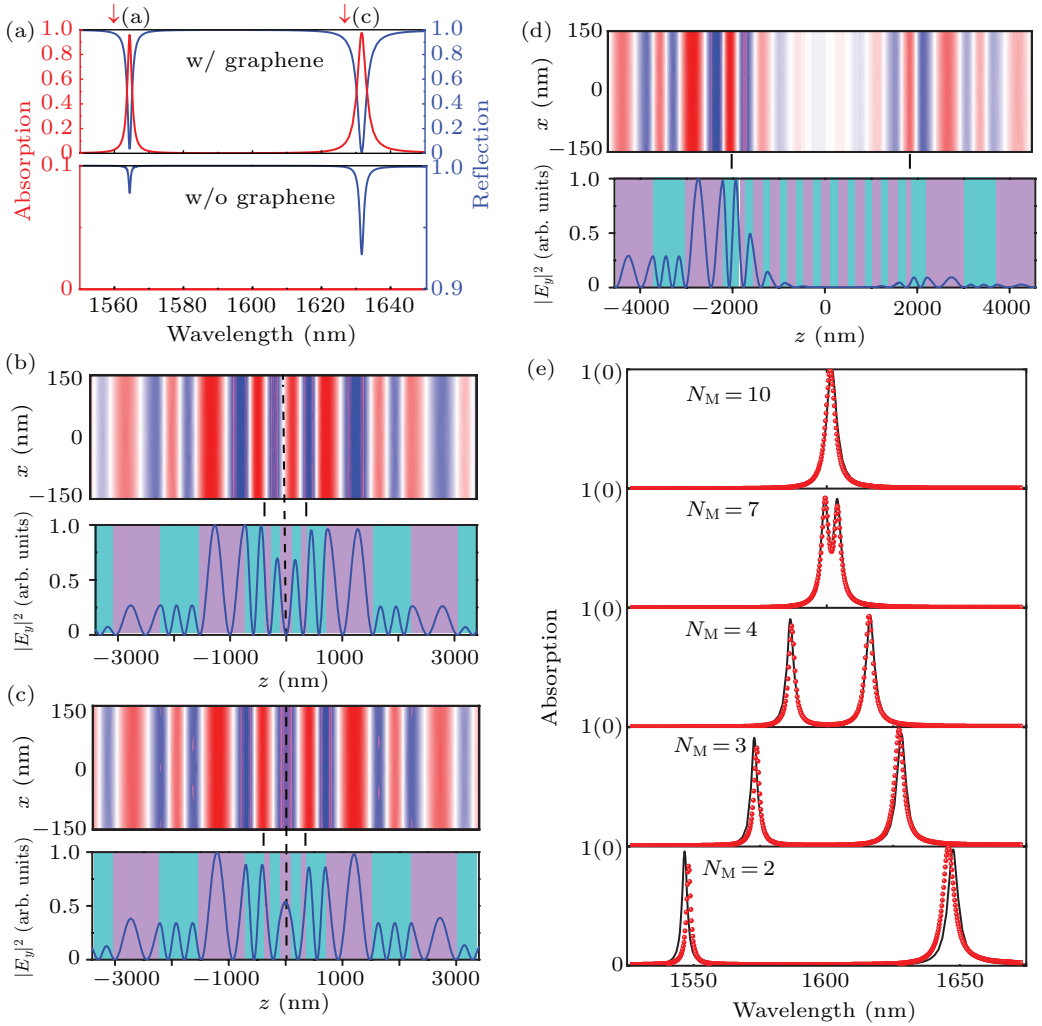


Fig. 3. (a) Comparison of absorption and reflection curves with and without graphene for the proposed structure. The electric field distribution of E_y and profile of $|E_y|^2$ at 1564.8 nm (b) and 1632 nm (c) with graphene when $N_M = 2$. (d) The electric field distribution of E_y and profile of $|E_y|^2$ at 1601.7 nm with graphene when $N_M = 10$. (e) Absorption curves at $N_M = 2$, 3, 4, 7, and 10 based on FEM (black lines) and TMM (red dots).

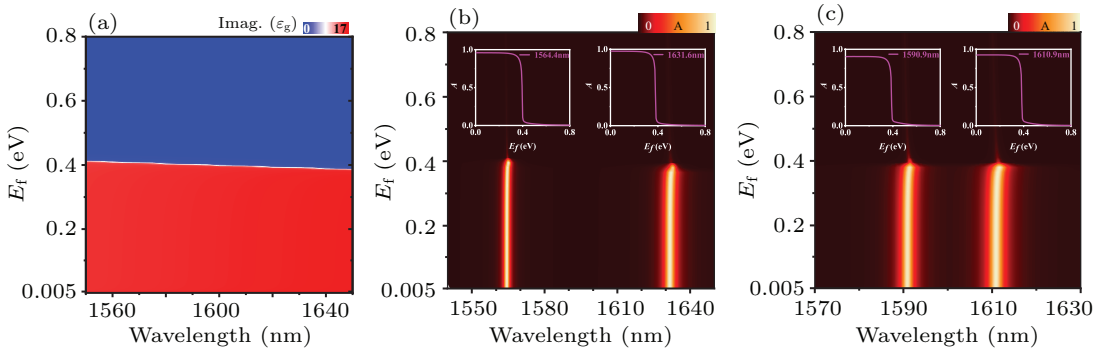


Fig. 4. (a) Imaginary parts of permittivity spectra of graphene with Fermi level. Absorption as a function of the wavelength and the Fermi level of graphene (E_f) when $N_M = 2$ (b) and 4 (c). The insets of (b) show absorption versus E_f at 1564.8 nm and 1632 nm, respectively. The insets of (c) show absorption versus E_f at 1591.3 nm and 1611.3 nm, respectively.

Finally, the influence of the incident angle θ on the dual-channel absorption is investigated for TE and TM polarization. Figures 5(a) and 5(c) show the absorption as a function of the wavelength and the incident angle θ for TE and TM polarization, respectively. The results calculated by TMM are also shown in Figs. 5(a) and 5(c) by cyan dots. The geometric parameters of the structure are the same as those used in Fig. 3(a). As shown in Figs. 5(b) and (d), for TE and TM po-

larization, the absorption curves at the incident angle θ is 0°, 5°, 10°, and 15° are calculated by FEM (solid lines) and TMM (dots), respectively. Obviously, it can be seen that the results obtained by FEM and TMM are identical. Due to the dependence of the gaps on the polarization and angle of incident light,[38] the change of the incident angle θ will have an impact on the overlap range of gaps for the TE or TM polarization. Here, For TE and TM polarizations, when the incident angle θ varies from 0° to 15°, the overlap range of gaps changes from 1500–1655 nm to 1380–1550 nm and 1500–1655 nm to 1400–1525 nm, respectively. Also, the blue shift for the coupled modes of TIS happens. For TE polarization, the wavelengths corresponding to the dual-channel absorption peaks vary from 1564.8 nm and 1632 nm to 1468.5 nm and 1525.4 nm. And the dual-channel absorption peaks both exceed 90% at θ of less than 8°. For TM polarization, the wavelengths corresponding to the dual-channel absorption peaks vary from 1564.8 nm and 1632 nm to 1443.5 nm and 1509.6 nm. And the dual-channel absorption peaks both exceed 90% at θ of less than 12°. Thus, the dual-channel absorption enhancement induced by coupled modes of TIS is robust and has a certain tolerance to incident angle for TE and TM polarization.

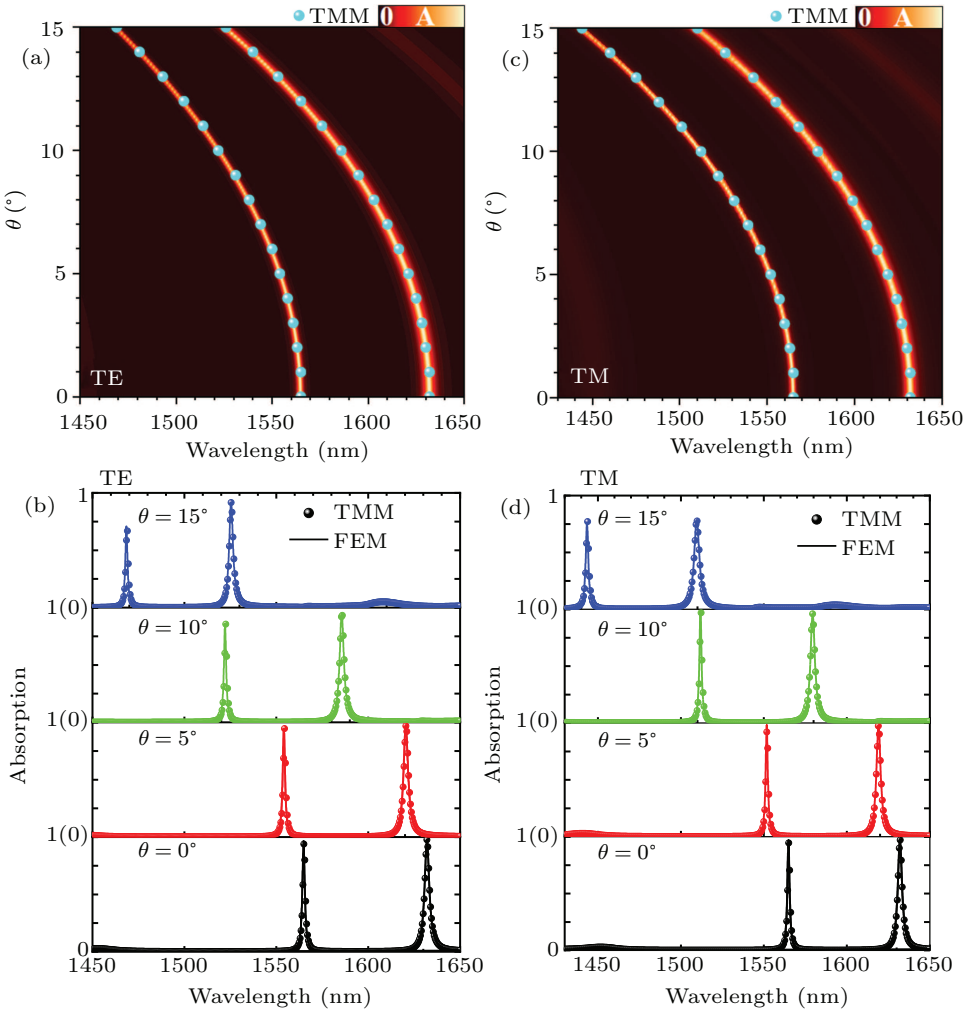


Fig. 5. Absorption as a function of the wavelength and the incident angle θ for TE (a) and TM (c) polarization, respectively. The cyan dots represent the results of TMM in (a) and (c). Absorption curves based on FEM (solid lines) and TMM (dots) at $\theta = 0°$, 5°, 10°, and 15° for TE (b) and TM (d) polarization.

3. Conclusion

In summary, an all-dielectric heterostructure consisting of PhC-F/graphene/PhC-M/graphene/PhC-B on GaAs substrate is proposed. TIS can be excited on the interfaces of PhC-F/PhC-M and PhC-M/PhC-B, where the coupled modes of TIS are generated through coupling between TIS. Due to the existence of the coupled modes of TIS, the highly localized electric field and energy at the interface promote the strong interaction between light and graphene, the dual-channel near-infrared absorption enhancement is realized. By increasing N_M, the dual-channel nearly perfect absorption can be modulated to single channel perfect absorption. The dual-channel absorption drops sharply by fine-tuning the Fermi level of graphene around 0.4 eV. Besides, the dual-channel absorption can be modulated by changing angle of incident light (TE and TM polarization). The simple all-dielectric layered system of the proposed heterostructure makes it promising for applications in optical absorbers, switches, sensing and modulators.

Acknowledgement

This project was supported by Postgraduate Research & Practice Innovation Program of Jiangsu Province, China (Grant No. KYCX20_1929).

References

[1] Yablonovitch E 1987 *Phys. Rev. Lett.* **58** 2059
[2] John S 1987 *Phys. Rev. Lett.* **58** 2486
[3] El-Naggar S A 2015 *Opt. Quant. Electron.* **47** 1627
[4] Joannopoulos J, Johnson S, Winn J and Meade R 2008 *Photonic Crystals: Molding the Flow of Light*, 2nd edn. (Princeton Univ.) p. 56
[5] Moghimi M, Mirzakuchaki S, Granpayeh N, Nozhat N and Darvish G 2012 *Can. J. Phys.* **90** 175
[6] Fan Y, Wei Z, Li H, Chen H and Soukoulis C M 2013 *Phys. Rev. B* **88** 241403
[7] Poshakinskiy A, Poddubny A, Pilozzi L and Ivchenko E 2014 *Phys. Rev. Lett.* **112** 107403
[8] Polini M, Guinea F, Lewenstein M, Manoharan H C and Pellegrini V 2013 *Nat. Nanotechnol.* **8** 625
[9] Lu L, Joannopoulos J D and Soljačić 2014 *Nat. Photonics* **8** 821
[10] Li C, Hu X, Gao W, Ao Y, Chu S, Yang H and Gong Q 2018 *Adv. Opt. Mater.* **6** 1701071
[11] Gao W, Hu X, Li C, Yang J, Chai Z, Xie J and Gong Q 2018 *Opt. Express* **26** 8634
[12] Liang Y, Xiang Y and Dai X 2020 *Opt. Express* **28** 24560
[13] Guo J, Wang H, Dai X, Xiang Y and Tang D 2019 *Opt. Express* **27** 32746
[14] Liu C H, Chang Y C, Norris T B and Zhong Z 2014 *Nat. Nanotechnol.* **9** 273
[15] Falkovsky L 2008 *J. Phys.: Conf. Ser.* **129** 012004
[16] Zhao B, Zhao J and Zhang Z 2014 *Appl. Phys. Lett.* **105** 031905
[17] Nikitin A Y, Guinea F, Garcia-Vidal F J and Martin-Moreno L 2012 *Phys. Rev. B* **85** 081405
[18] Thongrattanasiri S, Koppens F H and De Abajo F J G 2012 *Phys. Rev. Lett.* **108** 047401
[19] Nair R R, Blake P, Grigorenko A N, Novoselov K S, Booth T J, Stauber T, Peres N M and Geim A K 2008 *Science* **320** 1308
[20] Zhu X, Shi L, Schmidt M S, Boisen A, Hansen O, Zi J, Xiao S and Mortensen N A 2013 *Nano Lett.* **13** 4690
[21] Lu H, Gan X, Jia B, Mao D and Zhao J 2016 *Opt. Lett.* **41** 4743
[22] Wang X, Jiang X, You Q, Guo J, Dai X and Xiang Y 2017 *Photon. Res.* **5** 536
[23] Qing Y M, Ma H F and Cui T J 2019 *Opt. Lett.* **44** 3302
[24] Hu J, Liu W, Xie W, Zhang W, Yao E, Zhang Y and Zhan Q 2019 *Opt. Lett.* **44** 5642
[25] Lu H, Li Y, Yue Z, Mao D and Zhao J 2020 *Opt. Express* **28** 31893
[26] Wang X, Liang Y, Wu L, Guo J, Dai X and Xiang Y 2018 *Opt. Lett.* **43** 4256
[27] Zhang K, Liu Y, Xia F, Li S and Kong W 2020 *Opt. Lett.* **45** 3669
[28] Lin Y, Chou S and Hsueh W J 2020 *Opt. Lett.* **45** 4369
[29] Li Y, Lu H, Zheng J, Li S, Xuan X and Zhao J J 2021 *Chin. Opt. Lett.* **19** 103801
[30] Rakić A D and Majewski M L 1996 *J. Appl. Phys.* **80** 5909
[31] Su Z, Wang Y, Luo X, Luo H, Zhang C, Li M, Sang T and Yang G 2018 *Phys. Chem. Chem. Phys.* **20** 14357
[32] Xiao M, Zhang Z and Chan C T 2014 *Phys. Rev. X* **4** 021017
[33] Gao W, Xiao M, Chen B, Pun E Y, Chan C T and Tam W Y 2017 *Opt. Lett.* **42** 1500
[34] Dal Lago V, Atala M and Torres L F 2015 *Phys. Rev. A* **92** 023624
[35] Schmidt C, Palatnik A, Sudzius M, Meister S and Leo K J 2021 *Phys. Rev. B* **103** 085412
[36] Zhao Z, Li G, Su T, Yu F, Zhang Y, Wang W, Men W, Wang Z, Xuan L and Chen X 2019 *Opt. Express* **27** 35088
[37] Guo B, Fang L, Zhang B and Gong J R 2011 *Insciences J.* **1** 80
[38] Yeh D W and Wu C J 2009 *Opt. Express* **17** 16666